Characteristics of Stochastic Variability Associated with ENSO and the Role of the MJO

CRISPIAN BATSTONE*

School of Mathematics, University of East Anglia, Norwich, United Kingdom

HARRY H. HENDON

Bureau of Meteorology Research Centre, Melbourne, Australia

(Manuscript received 30 January 2004, in final form 6 September 2004)

ABSTRACT

To shed light onto the possible role of stochastic forcing of the El Niño–Southern Oscillation (ENSO), the characteristics of observed tropical atmospheric variability that is statistically uncoupled from slowly evolving sea surface temperature (SST) are diagnosed. The Madden–Julian oscillation (MJO) is shown to be the dominant mode of variability within these uncoupled or "stochastic" components. The dominance of the MJO is important because the MJO generates oceanic Kelvin waves and perturbs SST in the equatorial Pacific that may feed back onto the El Niño–Southern Oscillation. The seasonality present in the uncoupled zonal stress (maximum in austral summer), which reflects the seasonality of MJO activity, is also transmitted to the eastern Pacific thermocline variability by these Kelvin waves. Hence, the MJO component of the uncoupled stress could plausibly contribute to the observed phase locking of ENSO to the seasonal cycle.

During an El Niño event, maximum uncoupled zonal stress variance shifts eastward from the western Pacific along with the coupled surface westerly wind and warm SST anomalies. The MJO accounts for less than half of this low-frequency behavior of the uncoupled stress but accounts for nearly two-thirds of the resultant thermocline variability. The uncoupled zonal stress also exhibits weak, westerly anomalies in the western Pacific some 8–10 months prior to El Niño, which is mostly accounted for by the low-frequency (period $\gg$ 50 days) behavior of the MJO. This low-frequency behavior possibly explains why observed El Niño variability is recovered when weakly damped models are forced with similar estimates of observed stochastic zonal stress.

1. Introduction

The El Niño–Southern Oscillation (ENSO) is characterized by episodic oscillations in sea surface temperature (SST) and atmospheric winds and convection in the equatorial Pacific Ocean basin. ENSO's broad bandwidth (period 2–7 yr) and irregular variation in amplitude limit practical predictability to about a one-fourth cycle (~9 months). Recent modeling studies have pointed toward stochastic weather noise, uncoupled from the slowly evolving ocean, as a possible cause for the irregularity of ENSO. In simple models where the ENSO mode is unstable and periodic, introduction of stochastic forcing produces aperidocity (e.g., Blanke et al. 1997; Eckert and Latif 1997; Roulston and Neelin 2000). In other models where the ENSO mode is stable or slightly damped, stochastic forcing not only introduces irregularity but can also act to sustain the ENSO mode (e.g., Zavala-Garay et al. 2003). These interpretations of the role of noise in ENSO are dependent on both the models used and how the noise is defined. However, diagnostic analyses of observed SSTs (e.g., Penland and Sardeshmukh 1995), and subsurface temperatures (e.g., Kessler 2002) support the notion that the observed ENSO is a stable linear system driven by stochastic noise.

Stochastic atmospheric noise is typically defined as the variability that is independent of the slowly evolv-

* Current affiliation: Climate Diagnostics Center, Boulder, Colorado.

Corresponding author address: Dr. Harry Hendon, Bureau of Meteorology Research Centre, GPO Box 1289K, Melbourne 3001, Australia.
E-mail: hhh@bom.gov.au

ing SST associated with ENSO. Implicit is that stochastic variability results primarily from high-frequency atmospheric variability that is uncoupled from the underlying ocean. Some studies simplify the form of this noise by assuming that it varies randomly in time (i.e., displaying a white spectrum) but with spatial structure typical of the monthly mean wind variability that is incoherent with the SST (e.g., Blanke et al. 1997; Neelin et al. 2000). Using daily rather than monthly mean data, Zavala-Garay et al. (2003) estimate the observed noise to exhibit a red spectrum with a decorrelation time of a few days but otherwise no dominant time scale. In model studies where the ENSO dynamics behave linearly (e.g., Roulston and Neelin 2000; Zavala-Garay et al. 2003) the exact temporal variability of the noise is not overly important because it is only the occurrence of a low-frequency tail that allows the noise to directly project onto the ENSO mode. What is important, however, is that the noise possesses the large spatial scales and appropriate geographical distribution so that it can efficiently instigate ENSO events months in advance (e.g., Moore and Kleeman 1999).

Such idealized modeling studies, which employ simple (typically steady state) atmospheres, acknowledge that intraseasonal variability (uncoupled or coupled) is not explicitly simulated. The Madden–Julian oscillation (MJO), which is the dominant mode of intraseasonal variability over the tropical Indian and Pacific Oceans (e.g., Salby and Hendon 1994), may be especially relevant to ENSO because episodes of enhanced MJO activity act to increase the wind speed in the western equatorial Pacific (Shinoda and Hendon 2002). A low-frequency cooling that is conducive to the onset of El Niño (Kessler and Kleeman 2000) is possibly produced. Intraseasonal cooling of the western Pacific, induced by the cloudy–windy phase of the MJO, has also been associated with the initial eastward shift of warm water and convection at the onset of El Niño (Bergman et al. 2001). MJO-induced surface wind variations in the western Pacific also efficiently force equatorially trapped Kelvin waves (e.g., Kessler et al. 1995; Hendon et al. 1998), which can perturb the SST in the central and eastern Pacific through zonal advection and displacement of the thermocline (Kessler et al. 1995; Zhang 1997; McPhaden 2002). An individual MJO event has also been associated with the abrupt termination of El Niño (Takayabu et al. 1999). Furthermore, the MJO itself may be influenced by air–sea coupling (e.g., Wang and Xie 1998), which may make interaction with ENSO a complicated, nonlinear process.

Most studies of stochastic forcing of ENSO have also not considered any seasonality to the forcing or any systematic variation of the statistics of the forcing tied directly to the ENSO cycle. Intraseasonal surface variability is known to vary markedly both throughout the seasonal cycle and in association with ENSO. For instance, MJO activity near the equator is strongest near the equinoxes and overall activity is strongest during southern summer (Salby and Hendon 1994). Because ENSO itself is tightly tied to the annual cycle, the strong annual cycle of MJO activity might profoundly impact the manner in which MJO affects ENSO (Fedorov 2002; Fedorov et al. 2003). MJO activity is also observed to shift eastward into the central Pacific as El Niño develops (e.g., Hendon et al. 1999; Kessler 2001). This shift, which may simply be symptomatic of an eastward shift of warm water and convection on all time scales as El Niño develops, might also have predictive implications (e.g., Zhang and Gottschalck 2002).

The motivation for the present study is provided by previous model studies that have necessarily simplified the interaction between stochastic variability and ENSO. Rather than presume the spatial and temporal characteristics of the noise in order to be compatible with theories or models of ENSO, this study aims to diagnose more fully the spatial and temporal characteristics of the observed stochastic variability. In particular, we are interested in exploring the temporal and spatial spectrum of the stochastic variability on the full range of resolvable scales and how the observed stochastic variability evolves in relation to the ENSO cycle. Here, stochastic variability is defined as the atmospheric variability that is linearly unrelated to tropical Indo–Pacific SSTs at zero lag. It is important to point out that this definition of noise also includes variability that is not truly stochastic. For instance, variability that is nonlinearly related to SST will be attributed to the noise by this definition.

The remainder of the article proceeds as follows. The observational datasets, from which the coupled and stochastic atmospheric components are derived, are described in section 2. In section 3 the coupled and uncoupled (stochastic noise) atmospheric components are defined and their spatial and temporal characteristics are explored. The dominance of the MJO in the noise component is demonstrated in section 3. The response of the equatorial thermocline to forcing by the total noise and MJO components of zonal stress, which provides insight into how the noise may affect the evolution of ENSO, is provided in section 4. Discussion and conclusions are presented in section 5.

2. Data

Stochastic noise is defined here as atmospheric variability that is linearly unrelated to Indo–Pacific SST at zero lag. The rationale for this definition is that SST

evolves slowly and the atmospheric adjustment time to SST variations is short (on the order of a few days). Hence, noise can be defined as that part of the atmospheric variability that is not contemporaneously coherent with the SST. Atmospheric noise in both surface zonal wind, which has previously been identified as the most important component of stochastic forcing for ENSO in some models (e.g., Zavala-Garay et al. 2003), and deep convection is examined. Deep convection is considered because it is a fundamental component of the MJO and is also indicative of surface heat flux variations produced by the MJO (enhanced convection is associated with decreased shortwave radiation and enhanced latent heat flux; Shinoda et al. 1998). Here, outgoing longwave radiation (OLR) is used as a proxy for deep tropical convection. OLR data are available as daily averages interpolated to a 2.5° grid from National Oceanic and Atmospheric Administration (NOAA) polar-orbiting satellite observations (Liebmann and Smith 1996). Surface zonal wind data from the National Centers for Environmental Prediction–National Center for Atmospheric Research (NCEP–NCAR) reanalyses (Kalnay et al. 1996) are also available as daily averages on a 2.5° grid.

Atmosphere noise is defined with respect to weekly SSTs, which are the optimum interpolated analyses of Reynolds and Smith (1994). These weekly averages are interpolated to daily values to be compatible with the other datasets. The SST data are further restricted to the Indo–Pacific domain, 40°E−70°W, to emphasize the variability directly associated with ENSO. The SST and atmospheric data are used for the period 1 January 1982 to 31 December 1999 and truncated to the tropical domain, 30°N−30°S. Prior to all analysis, the annual, biannual, and triannual cycles and the time mean are removed to form daily anomalies.

3. Coupled and uncoupled atmospheric behavior

a. Tropical convection

To extract the component of an observed atmospheric field that is uncorrelated with Indo–Pacific SST, the coupled atmosphere–ocean component is first estimated (e.g., Blanke et al. 1997; Zavala-Garay et al. 2003). Here we define the coupled component by regressing atmospheric variability onto the leading empirical orthogonal functions (EOFs) of Indo–Pacific SST. We retain nine EOFs of SST, which account for 62% of the SST variance but most of the covariance with zonal wind and OLR (greater than 90% and 95%, respectively). The first EOF of SST, which accounts for 32% of the SST variance, depicts mature El Niño conditions, with positive loadings stretching westward along the equator from the west coast of South America and negative loadings in the far western Pacific (Fig. 1a). Its time series, or principal component (PC), shows large amplitude during the strong El Niño events of 1982/83 and 1997/98 (not shown). EOF2 accounts for 10% of the variance and explains variability concentrated more in the central Pacific Ocean (Fig. 1b). Its PC has maximum correlation with PC1 at a 10-month lead (0.46), thereby displaying precursory conditions to an El Niño event, with warming in the central Pacific Ocean. Higher-order EOFs exhibit more complicated horizontal structure and explain progressively less SST variance. However, because individual El Niño (and La Niña) events evolve in different ways, more than two EOFs are retained in order to describe more fully the evolution of slowly varying SST. A break in the SST eigenvalue scree plot, as defined using the criterion of North et al. (1982), between modes 9 and 10 also provides a natural cutoff for selection for the number of retained modes.

The coupled component of atmospheric variability is defined by the linear regression at each grid point, i, between the observed atmospheric anomaly field, y', and the PCs of the retained SST EOFs (e_j). The "statistically" coupled component (or "signal") of y' is then given by

$$\hat{y}_i(t) = \sum_j a_{i,j} + b_{i,j} e_j(t),$$

where the regression constants $a_{i,j}$ are zero as a result of the use of anomaly data. Because the principal components e_j are orthogonal in time (i.e., there is no cross correlation between the e_j), the regression coefficients $b_{i,j}$ are simply the univariate regression of y_i onto each e_j.

The regression of OLR onto EOF1 of SST, which accounts for ~84% of the covariability of OLR with SST, describes the large-scale convection anomalies associated with the mature phase of El Niño (Fig. 1a). Negative OLR near the date line reflects the eastward shift of the ascending branch of the Walker circulation from the Maritime Continent to the central Pacific Ocean (e.g., Prabhakara et al. 1985). Suppressed convection (positive OLR), associated with dry conditions in Indonesia and northern Australia characteristic of an El Niño event, occurs over the Maritime Continent. The coupled nature of the low-frequency variability in the tropical Pacific is also apparent in the regression of OLR onto the second SST PC, which accounts for about 7% of their covariance. Negative OLR anomalies reside over the warm SSTs in the central Pacific (Fig. 1b), alluding to the fact that anomalously warm tropical SSTs are more conducive to supporting deep tropical atmospheric convection.

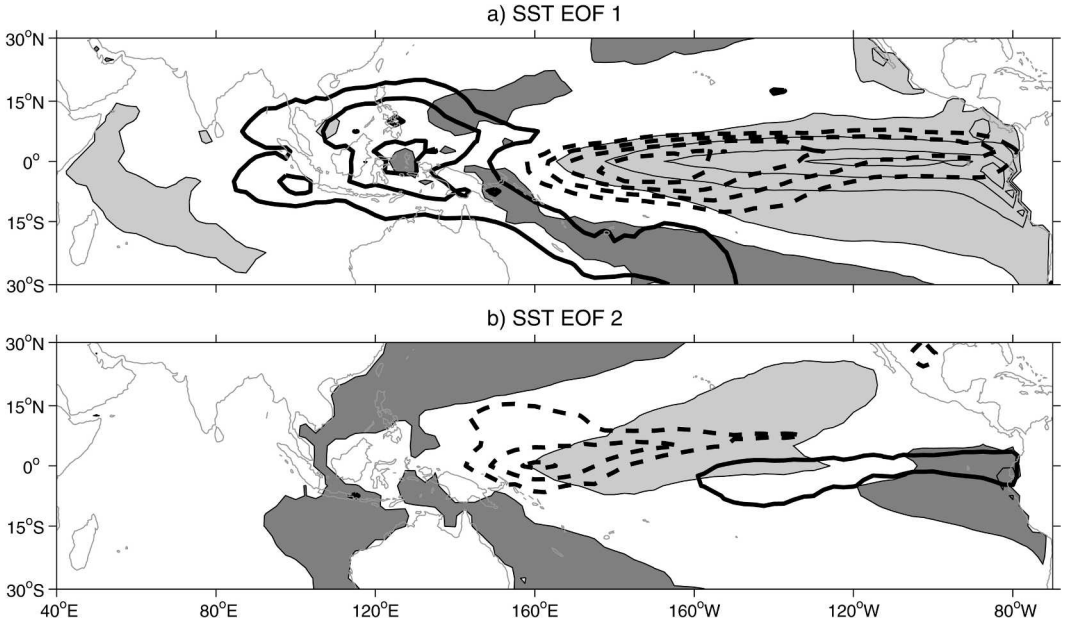

FIG. 1. EOFs 1 and 2 of SST anomaly (shading). Regression coefficients of OLR anomaly with the respective SST PCs are overlaid (contours). For SST, the shading interval is 0.4 K, with the first level at 0.2 K. Light (dark) shading indicates positive (negative) values. For OLR, the contour interval is 4 W m^{-2}, with negative values dashed and the zero contour omitted.

Summing the individual regressions over the nine retained SST PCs forms what we term the "coupled" component of OLR. These nine modes account for 96% of the covariability between the OLR and SST fields. The percentage of variability of the total OLR anomaly field explained by the coupled signal is large over the central and eastern equatorial Pacific Ocean (Fig. 2a), which is an area clearly dominated by ENSO variability. A coupled signal is also evident over the Maritime Continent, which is also an area where ENSO exerts significant influence (i.e., Indonesia typically experiences drought during El Niño). Interestingly, little coupled variability is evident in the Indian Ocean.

b. Uncoupled convective variability

Weather noise in this study is represented by the residual produced when the coupled component is subtracted from the original anomaly field. This residual is

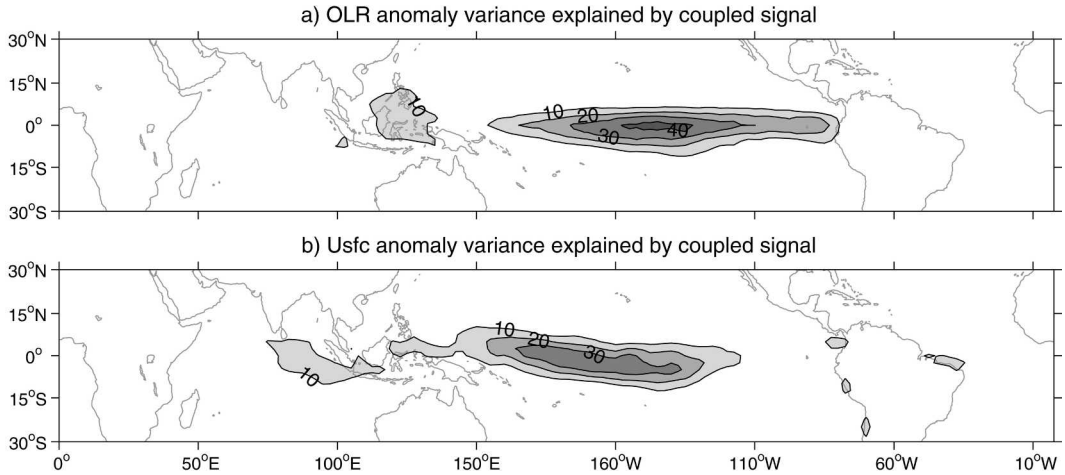

FIG. 2. Percentage of the total (a) OLR and (b) surface zonal wind anomaly variance explained by the respective coupled signal component. The contour interval is 10%.

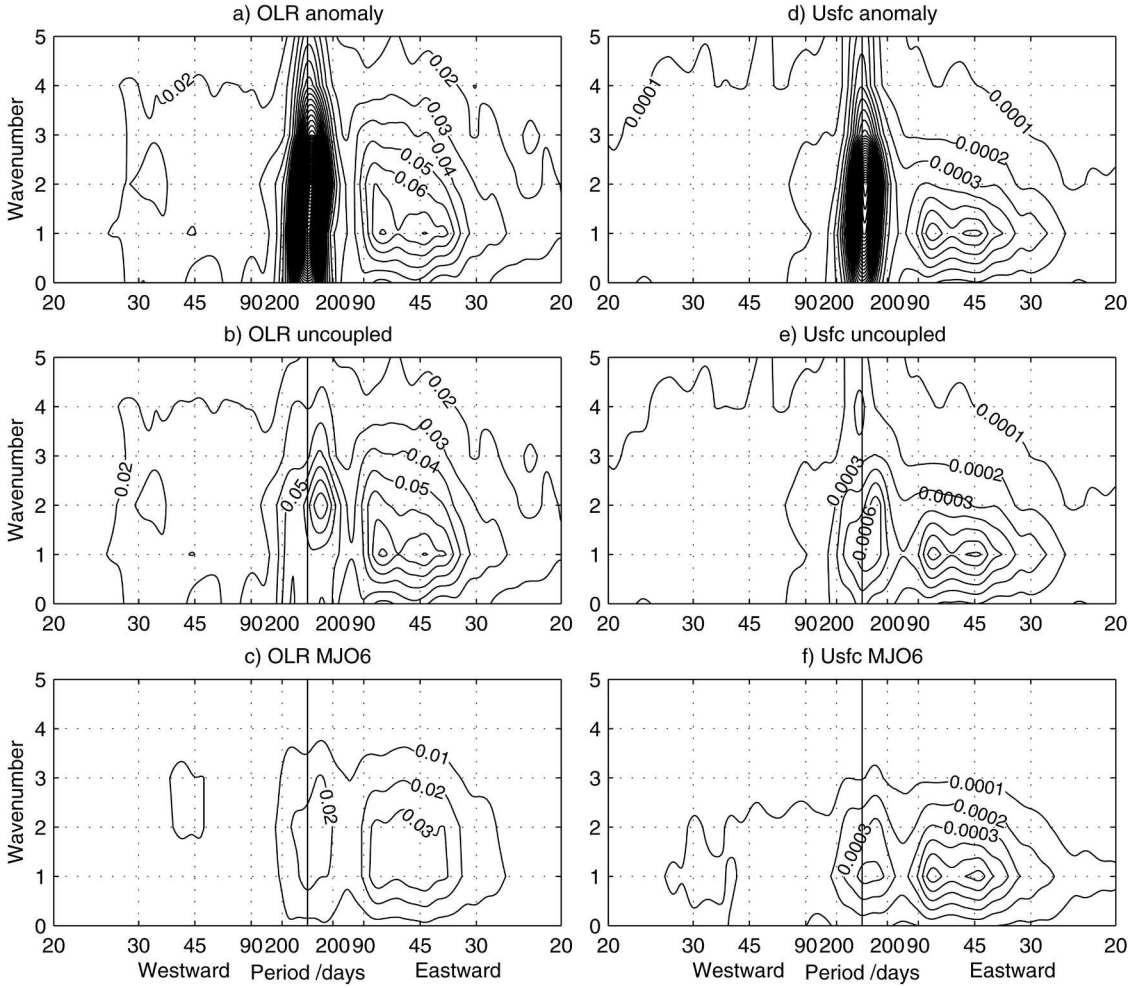

FIG. 3. Wavenumber–frequency spectra of (a) total OLR anomaly, (b) OLR uncoupled, and (c) OLR MJO6 component. (d)–(f) Spectra for the respective surface zonal wind components are also shown. Power is averaged in latitude between 10°N and 10°S and smoothed with 80 passes of 1/3–1/3–1/3 filter in frequency. For OLR, the contour interval is 0.01 $W^2\ m^{-4}$; for surface zonal wind, the contour interval is 0.0001 $m^2\ s^{-2}$.

termed the uncoupled component, or stochastic noise. Space–time spectra of the uncoupled and total OLR anomalies are computed in order to characterize the dominant time and space scales of variability. The power spectrum is computed at each latitude in the range 10°S–10°N and then averaged. Comparison of the spectra for total OLR anomaly and its noise component (Figs. 3a,b) shows that most low-frequency (periods longer than a season) variability is ascribed to the statistically coupled component (i.e., contemporaneously coherent with the slowly evolving SST). Hence, the uncoupled noise is dominated by the MJO, characterized by the spectral peak at eastward wavenumbers 1–2 and periods of 30–90 days. The MJO peak stands out above both red and white noise background spectra (e.g., Salby and Hendon 1994). Low-frequency power is also retained in the noise component, which, as discussed below, is partially accounted for by the low-frequency behavior of the MJO.

c. Surface zonal wind

Surface zonal wind is separated into coupled and uncoupled components using the same regression method. The coupled component (i.e., regression onto the leading nine EOFs of SST) accounts for 92% of the covariance between SST and zonal wind in the Indo–Pacific. Similar to OLR, the coupled component of surface zonal wind is largest in the equatorial western/central Pacific Ocean, which reflects the prominent eastward shift of westerly surface winds during El Niño (Fig. 2b). The uncoupled component of zonal wind is dominated by extratropical noise, which displays no preferred mode of variability (not shown; see also Zavala-Garay et al. 2003). However, as will be seen below, the near-

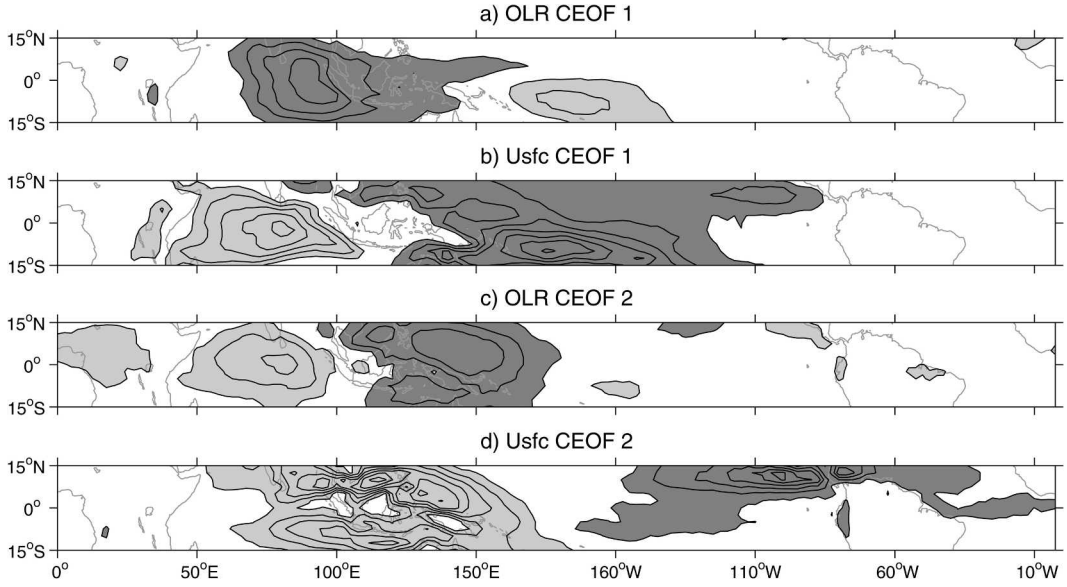

FIG. 4. (a) OLR CEOF1, (b) surface zonal wind CEOF1, (c) OLR CEOF2, and (d) surface zonal wind CEOF2 of a combined EOF analysis of the uncoupled OLR and surface zonal wind components (15°N–15°S). The contour interval is 0.01 with the zero contour omitted. Light (dark) shading indicates positive (negative) values.

equatorial uncoupled variability, which is more directly relevant to the evolution of ENSO, is dominated by the MJO.

The space–time spectrum of the total zonal wind anomaly field averaged about the equator (10°N–10°S), like that of OLR, exhibits greatest power at lowest frequencies, but again with an intraseasonal spectral peak associated with the MJO (eastward wavenumber 1 with period of 30–90 days; Fig. 3d). The uncoupled component retains the MJO signal while exhibiting reduced power at lower frequencies (Fig. 3e). As for the OLR, some low-frequency power, which will be shown to be partially accounted for by the low-frequency behavior of the MJO, is retained in the uncoupled component of the zonal wind. However, most of the low-frequency variability is ascribed to the coupled component.

d. MJO contribution

To demonstrate the dominance of the MJO in the uncoupled noise, the MJO component of the noise is objectively extracted by combined EOF analysis of the uncoupled OLR and surface zonal wind. Combined EOF (CEOF) analysis of near-equatorial OLR and zonal wind efficiently discriminates to the large-scale, overturning structure of the MJO (Wheeler and Hendon 2004). Prior to the EOF analysis, the individual fields are scaled by their respective root mean gridpoint variance. This is to ensure that both fields contribute equal total variance, preventing one field from biasing the analysis. Because the uncoupled component of surface zonal wind is dominated by extratropical noise that is not directly relevant to ENSO, the CEOF analysis is restricted to 15°N–15°S.

The leading pair of CEOFs portrays distinct MJO-like spatial and temporal behavior. CEOF1 displays large-scale enhanced convection across the eastern Indian Ocean (Fig. 4a), accompanied by large-scale surface zonal westerly (easterly) winds to the west (east) (Fig. 4b). CEOF2 exhibits similar structure (Figs. 4c,d) but shifted some 50° longitude east, suggesting that CEOFs 1 and 2 describe an eastward-propagating disturbance. This is confirmed by the squared coherence between their principal components, which peaks at over 0.6 in the 30–90-day band with a phase difference (PC1 leading PC2) of one-quarter cycle. Hence, CEOFs 1 and 2 capture much of the eastward-propagating variability associated with the MJO. However, the MJO exhibits year-to-year variability in zonal extent, especially during El Niño when it is displaced eastward in the Pacific. To capture this interannual variability, we need to retain higher-order CEOFs (e.g., Kessler 2001). Examination of the scree plot of the eigenvalues (not shown) reveals that modes 3 and 4 and 5 and 6 also appear as pairs (i.e., their eigenvalues are similar and their PCs are coherent in the 30–90-day band with a phase lag of one-quarter cycle), and they are separate from the following modes using the criterion of North et al. (1982). Modes 3–6 account for about 15% of the MJO spectral peak at eastward wavenumbers 1–3, with

periods of 30–90 days. Thus, we define the MJO component of the noise using the leading three pairs of CEOFs. Together, CEOFs 1–6 account for 16% of the total OLR–zonal wind variance.

The MJO components (referred to as MJO6) of the individual fields of OLR and surface zonal wind are formed by reconstruction using the leading six CEOFs. The fields are rescaled respectively using the retained values of root mean gridpoint variance. Space–time spectra reveal that MJO6 captures the majority of intraseasonal power at eastward wavenumbers that stands above the broad red background spectrum, including a prominent low-frequency (periods longer than 1 yr) tail (Figs. 3c,f). Interestingly, MJO6 captures more of the spectral peak associated with the MJO in the zonal wind than in the OLR. This suggests that the coupling between circulation and convection within the MJO is not completely robust, and MJO variability in OLR will therefore not be entirely represented in wind-coupled modes (and vice versa). Nevertheless, this definition of the MJO (the leading six CEOFs of OLR and zonal wind) effectively captures important aspects of MJO behavior relevant to the evolution of ENSO.

4. Dynamical ocean response

In this section, we examine the relation of the noise with the evolution of ENSO and infer what role the noise may play. The dominance of the MJO in the uncoupled noise implies that equatorial Kelvin waves will be efficiently excited (Kessler et al. 1995; Hendon et al. 1998). As they propagate into the eastern Pacific they may drive SST perturbations via anomalous zonal and vertical advection (e.g., Zhang 1997; McPhaden 2002), which may then influence the evolution of ENSO (e.g., Vecchi and Harrison 2000; Zhang and Gottschalck 2002). SST variations will also be directly driven in the western Pacific by the surface heat fluxes associated with the MJO (enhanced convection is associated with enhanced latent heat flux and decreased surface short wave radiation; e.g., Shinoda et al. 1998). These intraseasonal SST variations in the western Pacific, while not playing an important role in some simple models of ENSO (e.g., Zavala-Garay et al. 2003), have been implicated as important for the onset of some El Niño events (e.g., Bergman et al. 2001; Lengaigne et al. 2003). The MJO may also produce a rectified cooling of SST in the western Pacific because, over the life cycle of the MJO, the mean wind speed is increased (e.g., Kessler and Kleeman 2000; Shinoda and Hendon 2002). This cooling can help reverse the local zonal SST gradient, thereby promoting westerlies in the western Pacific, conducive to onset of El Niño.

a. Linear thermocline response

One way to explore how the uncoupled noise may drive a response in the ocean that is relevant to the evolution of ENSO is to force a linear shallow-water model of the Pacific basin (Burgers et al. 2002) with the zonal stress component of the noise. Previous studies suggest that the shallow-water model adequately simulates observed intraseasonal thermocline variability when forced with observed intraseasonal zonal stress (e.g., Hendon et al. 1998; Bergman et al. 2001). The simulated thermocline variability can also be thought of as being equivalent to filtering the zonal stress to those time and space scales that project onto the equatorial wave modes. This exercise is an extension of the study by Zhang and Gottschalck (2002), who considered just the Kelvin wave response to zonal stress variations produced by the MJO. Here, we consider all of the noise forcing and the full spectrum of the response.

To force the linear shallow water, uncoupled zonal stress is simply estimated from the uncoupled surface zonal wind using a bulk formula:

$$\tau = \rho_a C_D \overline{V} u_{\text{stoc}},$$

where $\rho_a = 1.17\ \text{kg m}^{-3}$, $C_D = 1.5 \times 10^{-3}$, and the mean surface wind speed $\overline{V}$ is specified as $5\ \text{m s}^{-1}$, which is typical over the domain of study. The shallow water wave speed, c_0, is set at $2.2\ \text{m s}^{-1}$, which is adequate to account for most of the observed interannual variation (Philander 1990) and gives the best representation of intraseasonal variations (Hendon et al. 1998) in the equatorial Pacific Ocean. However, Harrison and Giese (1988) argue that higher internal modes (slower phase speeds) are excited by synoptic-scale westerly wind events; hence this simple model may not capture the full dynamical response to the noise forcing. Realistic coastal boundaries are included at the eastern and western edges of the domain, with latitudinal boundaries at 30°N and 30°S that act as sponge layers. The horizontal resolution is 1° latitude by 2° longitude. A time step of 6 h is used to which the daily stress is interpolated. Here we concentrate on the simulated depth perturbation, which we equate to the observed thermocline variations. To assess the role of the MJO component of the noise, the model is forced with both the total uncoupled noise and just the MJO6 component.

b. Characteristics of the noise and oceanic response

Figure 5 displays a representative example of the uncoupled zonal stress and the shallow-water response along the equator for the period 1996–99. This period covers the growth and decay of the major El Niño event of 1997/98, which is seen in the contours of the observed

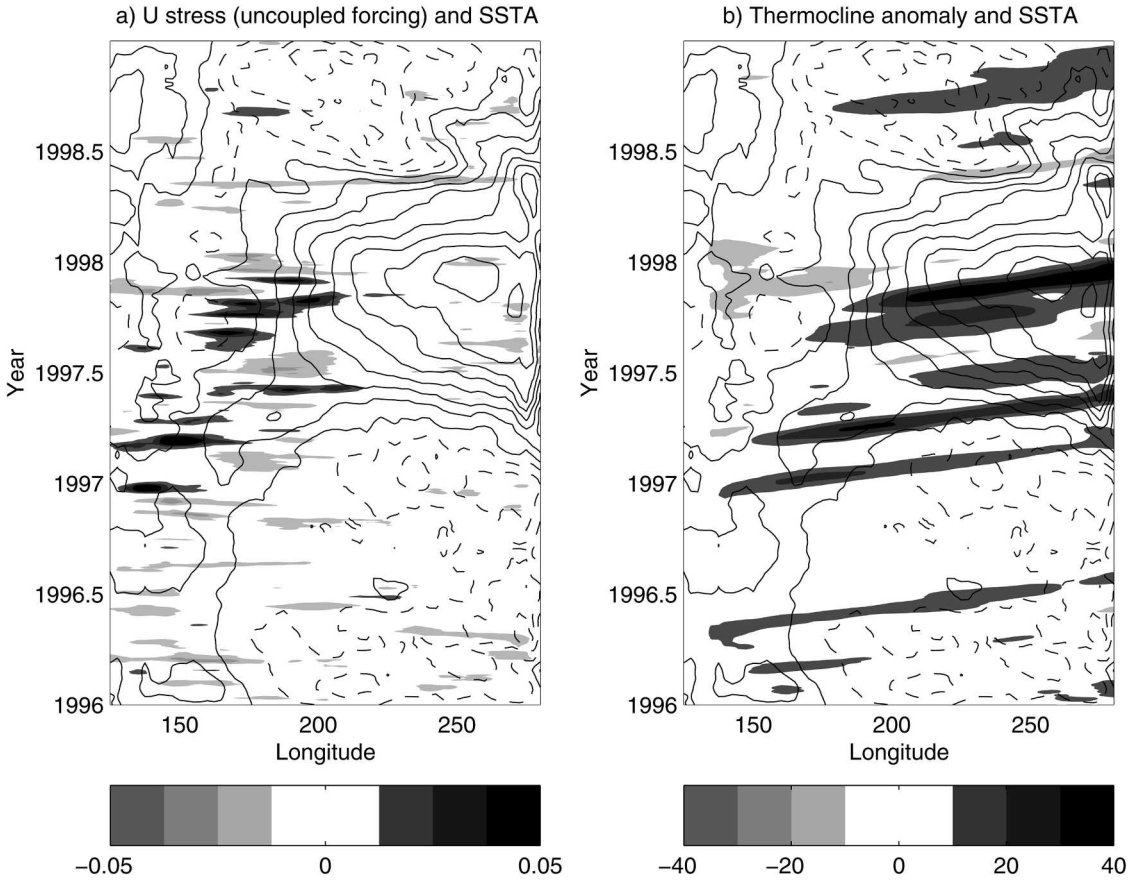

FIG. 5. Time–longitude diagrams of (a) uncoupled surface zonal stress and (b) simulated thermocline response for the period 1996–99 (shading). Observed SST anomalies are overlaid (contours). Values are averaged in latitude between 5°N and 5°S. The shading interval for stress is 0.01 N m^{-2} and for the thermocline it is 5 m. The contour interval for SST is 0.5 K with negative values dashed. A 14-day running mean filter is applied to the stress and thermocline anomalies, and a 50-day running mean filter is applied to the SST anomaly.

SST anomalies. As anticipated, the uncoupled zonal stress (Fig. 5a) is dominated by intraseasonal variations typical of the MJO, and pulses of intraseasonal Kelvin waves dominate the thermocline response (Fig. 5b). Episodes of westerly (easterly) surface stress in the western Pacific force downwelling (upwelling) equatorial Kelvin waves that propagate freely into the eastern Pacific. Some interesting low-frequency variations are also apparent. Prior to the peak of El Niño at the end of 1997, intraseasonal fluctuations in uncoupled surface stress in the western Pacific occur more frequently and successively farther to the east. This is reflected by increased Kelvin wave activity to the east. This increase and eastward shift of intraseasonal zonal stress variability prior to the peak of El Niño, which has been attributed to the behavior of the MJO (e.g., Kessler 2001), will be further diagnosed below. Also apparent in Fig. 5 is a net westerly stress forcing in the west (more positive than negative zonal stress anomalies) for the first 9 months of 1997 and an associated net thermocline deepening in the east prior to the peak of El Niño in late 1997. The appearance of a net westerly stress in the west (and its associated net deepening of the thermocline in the east) some 6–12 months prior to the peak of EL Niño has important ramifications for the role of the noise in the evolution of El Niño (e.g., Zavala-Garay et al. 2003). This too will be further explored below.

The spatial distribution of thermocline variance driven by the zonal stress noise (Fig. 6a) is consistent with the dominance of Kelvin wave activity: maximum variance occurs within 5° latitude of the equator in the central and eastern Pacific. However, off-equatorial maxima in the far western and far eastern Pacific indicate the presence of some Rossby wave activity. This model thermocline variability also resembles that derived from observations (Meinen and McPhaden 2000). As anticipated, the MJO component of the noise forcing accounts for the majority (60%–70%) of the equatorial variance (Fig. 6b).

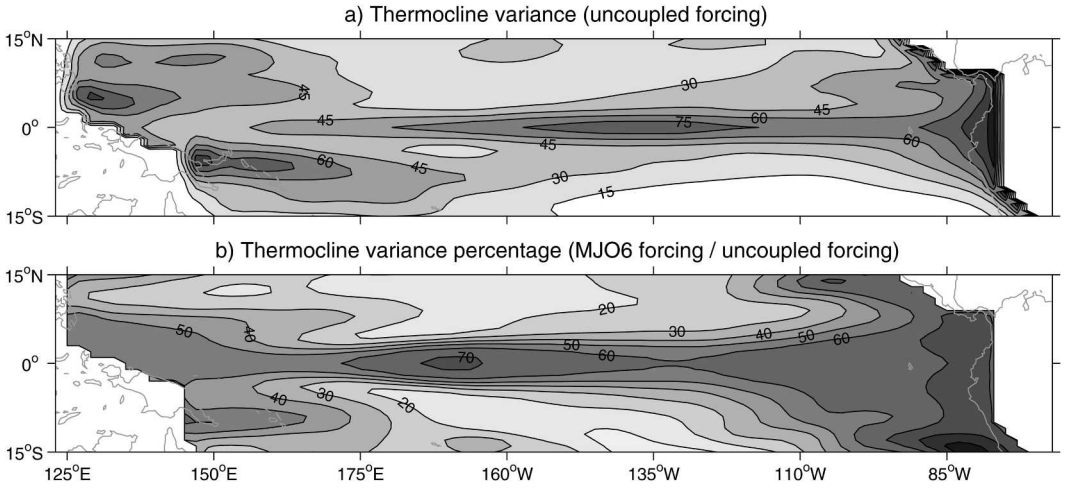

FIG. 6. (a) Simulated thermocline variance forced by uncoupled surface zonal stress. The contour interval is 15 m^2. (b) Percentage of thermocline variance due to MJO6 component of stress. The contour interval is 10%.

The predominance of Kelvin wave activity excited by the zonal stress noise is further demonstrated by the wavenumber–frequency spectrum of equatorial thermocline variability (Fig. 7a). This spectrum was generated by "padding" the thermocline anomalies from the Pacific domain with zeros in order to create an artificial periodic global domain. Maximum power falls along the Kelvin wave dispersion curve $\omega/k = 2.2\ \mathrm{m\ s^{-1}}$, with a peak near 75 days and a dropoff in power for periods less than about 40 days. The abrupt dropoff around 40 days occurs despite the fact that the uncoupled zonal wind has large eastward power down to about 30 days (Fig. 3e). The large spatial coherence of the stress at these frequencies (i.e., large power at zonal wavenumbers 1 and 2) results in this abrupt high-frequency cutoff (Kessler et al. 1995). The peak in the response near 75 days is indicative of near-resonant forcing of the Kelvin waves by the lower-frequency components of the eastward-propagating MJO (Hendon et al. 1998). The spectrum of thermocline variability forced by just the MJO6 component of zonal stress (Fig. 7b) confirms that almost all Kelvin wave power can be attributed to forcing by the MJO.

Large power is also evident at eastward low frequencies (periods longer than 200 days). This low-frequency power is peaked at zonal wavenumbers 1–2 and is at lower frequency than the gravest Kelvin wave in the Pacific basin (i.e., zonal wavenumber 3 with wavelength ~13 300 km), indicating that the forcing itself exhibits this characteristic. Interestingly, the MJO component

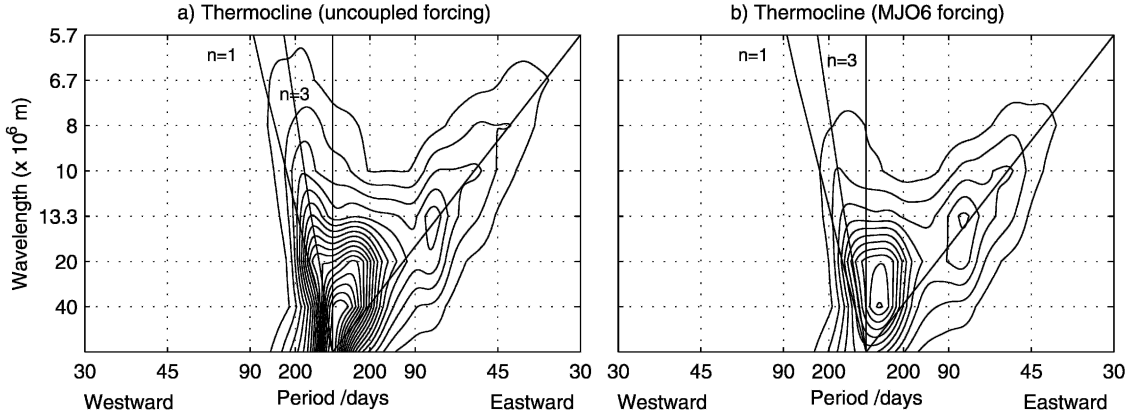

FIG. 7. Wavenumber–frequency spectra of the simulated thermocline forced by the (a) uncoupled and (b) MJO6 component of surface zonal stress. Power is averaged in latitude between 4°N and 4°S and smoothed with 80 passes of 1/3–1/3–1/3 filter in frequency. Phase speed lines for Kelvin wave ($\omega/k = 2.2\ \mathrm{m\ s^{-1}}$) and the first two symmetric Rossby waves (1 and 3) are included. The contour interval is $2 \times 10^{-3}\ \mathrm{m^2}$.

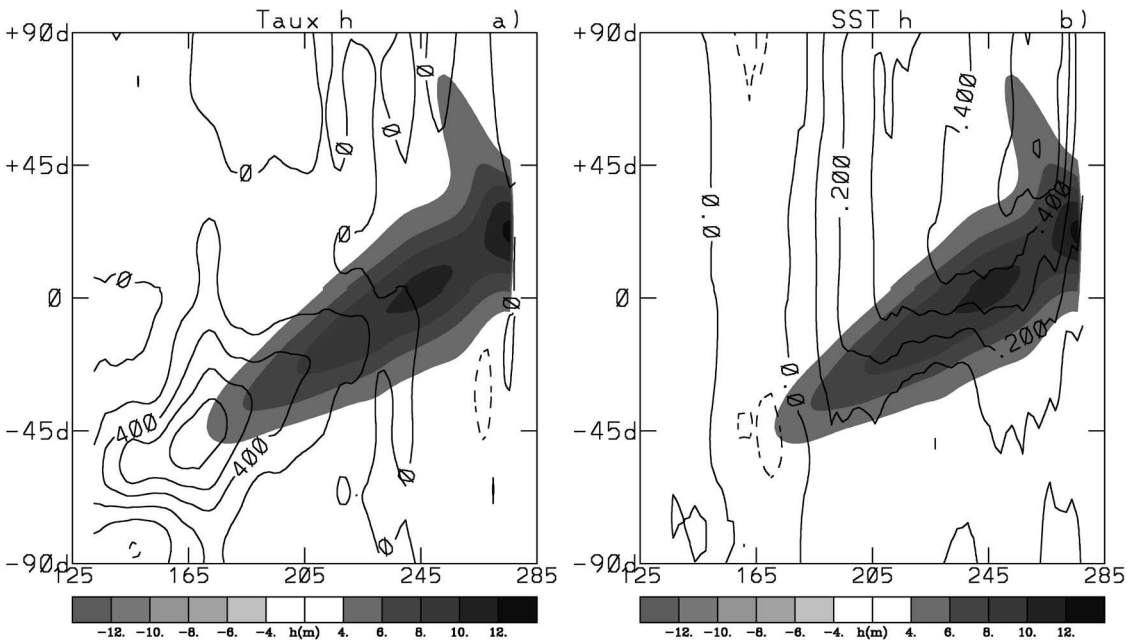

FIG. 8. Regressions of (a) uncoupled zonal stress (contours) and simulated thermocline depth (shading) and (b) observed SST (contours) and simulated thermocline depth (shading) onto the simulated thermocline depth between 110° and 120°W. Fields are averaged in latitude between 5°N and 5°S, and a 14-day running mean is applied prior to the regressions. Contour intervals are 2×10^{-3} N m^{-2} and 0.1 K for zonal stress and SST, respectively. The shading level for thermocline depth is 2 m.

of the forcing produces a similar low-frequency peak (Fig. 7b), even though power at these low frequencies in the stress forcing is much smaller than at intraseasonal frequencies (Fig. 3f). This results from the more efficient response of the ocean to lower frequencies (Kessler et al. 1995) and again emphasizes the potential importance of the low-frequency tail of the noise for the coupled climate system.

Significant westward power at low frequencies is also generated by the zonal stress noise (Fig. 7a). This power falls along the dispersion curves for the gravest symmetric equatorial Rossby waves (e.g., Gill 1982). The gravest symmetric Rossby wave ($n = 1$) has a phase speed approximately one-third of the Kelvin wave (i.e., ~0.7 m s^{-1}), while the phase speed of the next symmetric mode ($n = 3$) is even slower (i.e., ~0.3 m s^{-1}). Higher-order Rossby waves, whose maximum thermocline variability occurs farther off of the equator, are presumably excited because the zonal stress noise monotonically increases with latitude. Inspection of the thermocline response along the equator and 5°N for specific periods (not shown) also reveals obvious Rossby wave generation from reflection of Kelvin waves at the eastern boundary as well as from direct stress forcing in the interior of the domain. While the Rossby waves, as a result of their lower frequency, may be important for slow variations of ENSO (e.g., Jin 2001), the focus here is on the more dominant equatorial Kelvin waves.

More evidence for the dominance of the Kelvin waves in the thermocline response and for the manner in which they are forced is gained by computing lagged regression with respect to the thermocline perturbation in the equatorial eastern Pacific (Fig. 8). Thermocline variability there is dominated by an apparent intraseasonal Kelvin wave that has propagated in from the western Pacific, where it was forced by westerly stress some 40–60 days earlier (Fig. 8a). The stress anomaly has characteristics of the MJO (eastward propagating with a zonal half wavelength of ~70°–80°), but the local period and eastward phase speed are on the low side (~80 days and ~2–3 m s^{-1}) for a typical MJO. Despite the occurrence of maximum stress variance at the typical MJO periods (40–50 days), the equatorial thermocline acts as a low-pass filter, responding preferentially to the slower and lower frequency components of the MJO (Kessler et al. 1995; Hendon et al. 1998).

Observed SST is also regressed onto the thermocline perturbation in the east Pacific. Upon arrival of the downwelling Kelvin wave in the eastern Pacific, observed SST warms (Fig. 8b). This behavior is also evident for individual Kelvin waves as shown, for example, in Fig. 5. Maximum warming (or cooling in the case of the upwelling Kelvin wave) coincides with maximum

thermocline suppression. Implied then is that the warming is being driven by either anomalous zonal advection of the mean SST gradient (maximum anomalous eastward current coincides with maximum thermocline suppression for a Kelvin wave) or vertical advection of the anomalous vertical temperature gradient by mean upwelling (Zhang 1997; McPhaden 2002). Vertical advection of the mean vertical temperature gradient by the anomalous vertical motion associated with the Kelvin wave can be ruled out because it would produce a temperature tendency that leads the thermocline perturbation by one-quarter cycle. The peak SST anomaly in the eastern Pacific thus occurs some 70–90 days after the peak westerly stress anomaly appears in the western Pacific. Vecchi and Harrison (2000) obtained a similar result based on composites of westerly wind events in the western Pacific. However, the results here emphasize that it is a particular temporal and spatial structure of the zonal stress anomalies in the western Pacific (i.e., similar to the MJO) that allows Kelvin waves to be efficiently excited; they then communicate their impact into the eastern Pacific.

This effective bandpass filtering of the surface zonal wind by the ocean is confirmed by regression of simulated thermocline depth, uncoupled zonal stress, and observed SST anomalies directly onto the uncoupled zonal stress in the western Pacific (155°–165°E; not shown). While the stress variation now exhibits a higher frequency more in line with the dominant MJO period, it is associated with a much weaker Kelvin wave and resultant SST anomaly in the eastern Pacific. Hence, it is the low-frequency tail of the eastward-propagating MJO that allows for efficient excitation of Kelvin waves, which then can perturb the SST in the eastern Pacific.

It is also interesting to note that the SST variation associated with the arrival of the Kelvin wave in the eastern Pacific (Fig. 8b) shows a distinct asymmetry about zero lag. That is, little SST of opposite sign is observed before the arrival of the Kelvin wave, and the SST anomaly persists longer than the half period of the Kelvin wave (see also Vecchi and Harrison 2000). Harrison and Giese (1988) argue that higher vertical mode Kelvin waves and nonlinear interactions with instability waves can promote such a low-frequency response to episodic forcing in the western Pacific. These characteristics may also be indicative of some sort of locally coupled response, though untangling it from the slower evolution of ENSO may not be possible. Note also that the regressions in Fig. 8 have been scaled for a 1.5 standard deviation thermocline perturbation in the eastern Pacific. Because we use a linear model to derive the thermocline fluctuations from the observed zonal winds and we use a simple linear relationship to estimate the zonal stress anomalies from the zonal wind anomalies, the magnitude of the thermocline variations cannot be taken too seriously. However, their amplitude is realistic (e.g., Kessler et al. 1995; Hendon et al. 1998). Thus, a 10–12-m simulated thermocline perturbation results from an observed 0.8×10^{-2} N m^{-2} stress perturbation in the western Pacific and is associated with an observed 0.5-K warming in the eastern Pacific.

MJO activity is known to exhibit a distinct annual cycle, with weakest activity occurring during northern summer and strongest activity during southern summer (e.g., Salby and Hendon 1994). The dominance of the MJO in the zonal stress noise implies a prominent annual cycle in the thermocline response. This is confirmed by examining the annual cycle (retaining the first three harmonics of the annual cycle) of variance of the zonal stress noise in the western Pacific, which exhibits a maximum from October through April and a distinct minimum from June through September (Fig. 9). Similarly, the resultant thermocline variance in the central and eastern Pacific is a maximum from October through March and is a minimum in August and September. This pronounced seasonality of the zonal stress noise and its accompanying response in the thermocline has not been considered in some studies of the impact of noise on ENSO (e.g., Blanke et al. 1997; Neelin et al. 2000; Thompson and Battisti 2000). The results of Fedorov (2002) imply that it may be important because the impact of stochastic wind forcing on the evolution of ENSO is dependent on the state of ENSO, which itself is tightly tied to the seasonal cycle.

c. Relationship with ENSO

To this point we have shown that uncoupled atmospheric variability is dominated by intraseasonal variations associated with the MJO. Intraseasonal oceanic Kelvin waves are efficiently excited by the zonal stress component of this noise. The noise also contains low-frequency variations (i.e., periods longer than 200 days), some of which can be attributed to the low-frequency behavior of the MJO. This low-frequency tail of the noise may be of particular importance to the evolution of ENSO because it is especially efficient at producing a low-frequency response in the thermocline. Here we explore in more detail how the noise evolves through the ENSO cycle.

To examine the evolution of noise through the ENSO cycle, we regress the variance of zonal stress (total uncoupled and MJO6 component) and resulting thermocline variances onto the Niño-3 index (Fig. 10). Prior to the regression, variances were computed in a

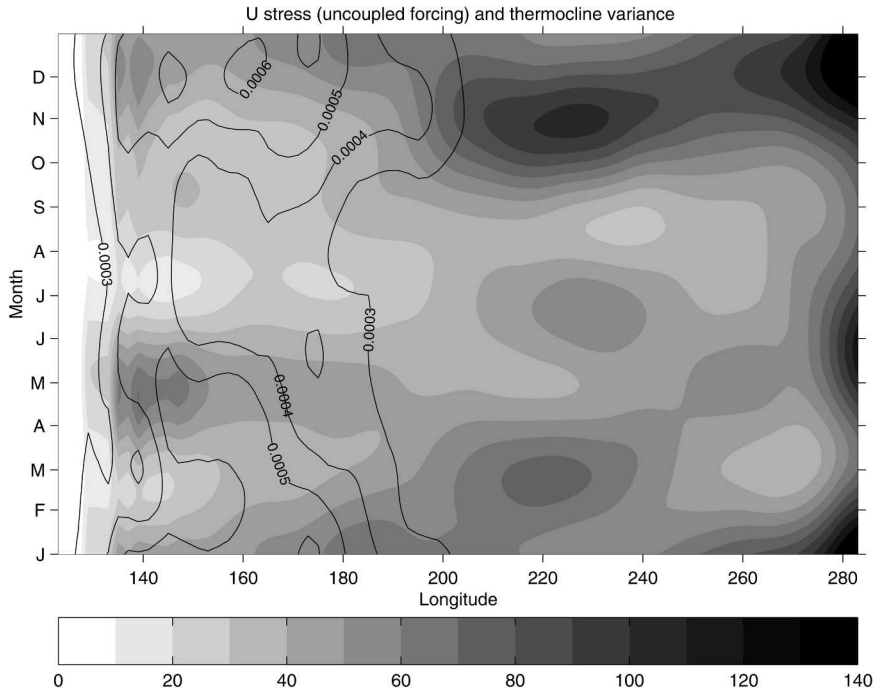

FIG. 9. Time–longitude diagram of the mean annual cycle of uncoupled zonal stress variance (contours) and simulated thermocline variance (shading). Values are averaged in latitude between 5°N and 5°S. The shading level for thermocline variance is 15 m^2, and the contour interval for stress variance is 1×10^{-4} N^2 m^{-4}, with the first contour at 3×10^{-4} N^2 m^{-4}.

running 90-day window, and the mean annual cycle of the variance was then removed. All fields were averaged between 5°N and 5°S. For reference, we also show the regression of *coupled* zonal stress and the correlation of SST onto the Niño-3 index (correlation rather than regression is shown in order to emphasize the negative SST anomalies in the far western Pacific; Fig. 11). For the 18-yr period considered here (1982–99), coupled westerly stress anomalies first appear in the western Pacific some 8–12 months prior to the peak of El Niño (Fig. 11). They appear just west of a positive SST anomaly centered near 165°E, which is the typical precursor to El Niño during this period. As El Niño matures, westerly stress anomalies intensify and slowly drift eastward, peaking near the date line in conjunction with warm SSTs in the eastern Pacific at lag 0. The initial SST adjustment in the eastern Pacific is much more rapid than this slow eastward drift of the stress anomalies, indicative of the arrival of the downwelling Kelvin wave front generated by the initial westerly anomalies at lags of 8–12 months. As the westerly stress anomaly drifts slowly eastward, cold SSTs develop west of 165°E. The initial cooling in the far western Pacific in conjunction with enhanced westerly winds (lag –8 months) has been associated with the initial intensification of El Niño events (e.g., Bergman et al. 2001; Lengaigne et al. 2003).

The evolution of uncoupled and MJO6 zonal stress *variance* (Figs. 10a,b) mimics the eastward expansion of the coupled westerly stress anomaly (Fig. 11). Initially, enhanced uncoupled (and MJO6) zonal stress variability is confined to the far western Pacific (lags –10 to –8 months). This is consistent with Zhang and Gottschalck (2002), who find increased MJO activity in the western Pacific Ocean some 8 months prior to the peak of Niño-3. As El Niño develops, the uncoupled stress variance shifts eastward in conjunction with the coupled westerly zonal stress anomaly. Beginning at lag 0, decreased noise stress variability develops in the far western Pacific. This eastward displacement of the MJO6 zonal stress variance at the mature phase of El Niño is consistent with observations of MJO activity shifting eastward during El Niño (Hendon et al. 1999; Kessler 2001).

Associated with the eastward intensification of uncoupled stress variance as El Niño develops, noise-forced thermocline variance intensifies and expands eastward, peaking 1–2 months prior to Niño-3 (Fig. 10). The thermocline variance driven by the MJO6 component of the stress, while only about one-third the mag-

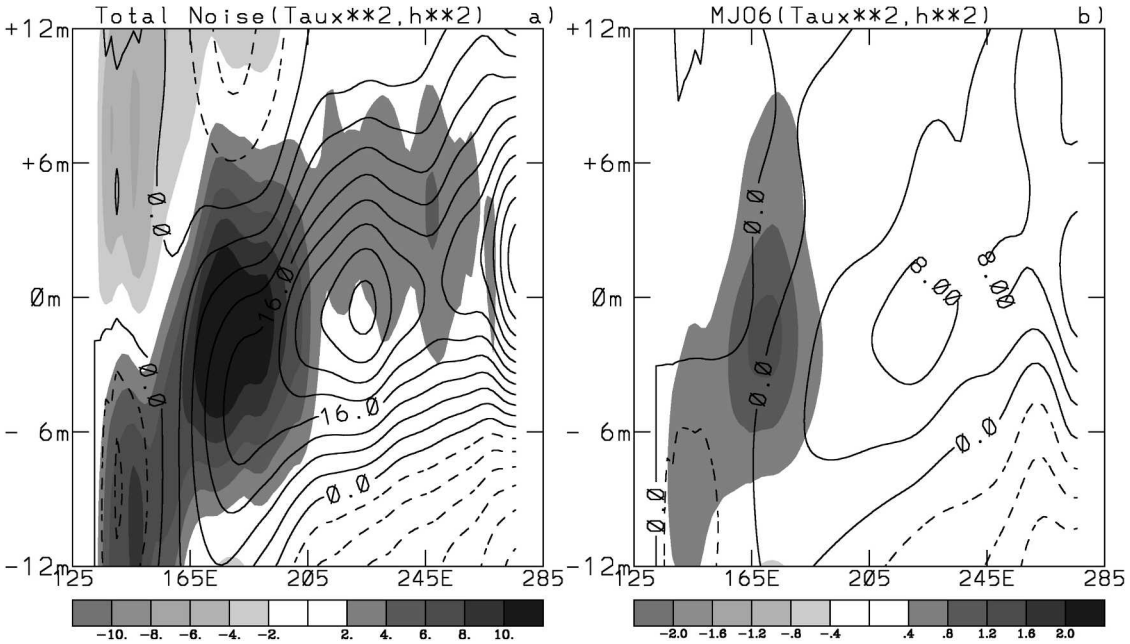

FIG. 10. Regression of (a) uncoupled zonal stress *variance* (shading) and resultant model thermocline *variance* (contours) and (b) MJO6 zonal stress variance (shading) and resultant model thermocline variance (contours) onto Niño-3. Fields are averaged between 5°N and 5°S, and a 90-day running mean is applied prior to the regression. The contour interval is 4 m^2 for thermocline variance. The shading level for zonal stress variance is 2×10^{-5} N^2 m^{-4} in (a) and 4×10^{-6} N^2 m^{-4} in (b).

nitude of the total, also shows this eastward intensification that peaks just before Niño-3. The development of maximum thermocline variability near the date line some 6–8 months prior to the peak of Niño-3 is consistent with the findings of Zhang and Gottschalck (2002). However, we diagnose peak noise-forced thermocline variability to continue to move eastward to near 150°W and peak about 1 month prior to the peak of El Niño. This discrepancy may be explained because Zhang and Gottschalck considered the Kelvin wave response to only MJO forcing, which they define using only two pairs of EOFs. Hence, they may have missed some of the interannual eastward displacement of intraseasonal zonal stress. It is not clear, however, whether the evolution of the noise, which simply tracks the evolution of warm SST and anomalous westerly stress, is simply a reflection of the slow SST evolution or whether the characteristics of the noise are determining the slow SST evolution.

The above analysis emphasizes how uncoupled zonal stress variability evolves with ENSO. This view is important if, for instance, it is the increase or decrease in atmospheric noise variability that leads to a rectified response in the coupled system (e.g., Kessler and Kleeman 2000; Shinoda and Hendon 2002). On the other hand, some studies have indicated that it is not the intraseasonal variations of circulation and SST pro-

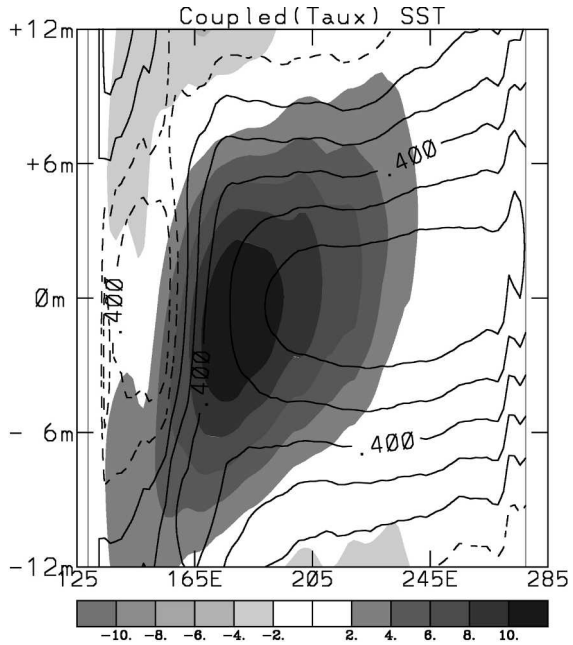

FIG. 11. Regression of coupled zonal stress (shading) and correlation of observed SST anomaly (contours) anomalies onto Niño-3. Fields are averaged between 5°N and 5°S, and a 90-day running mean is applied prior to the regression. The SST correlation is contoured with interval 0.2. For zonal stress anomaly, the contour interval is 2×10^{-3} N m^{-2}.

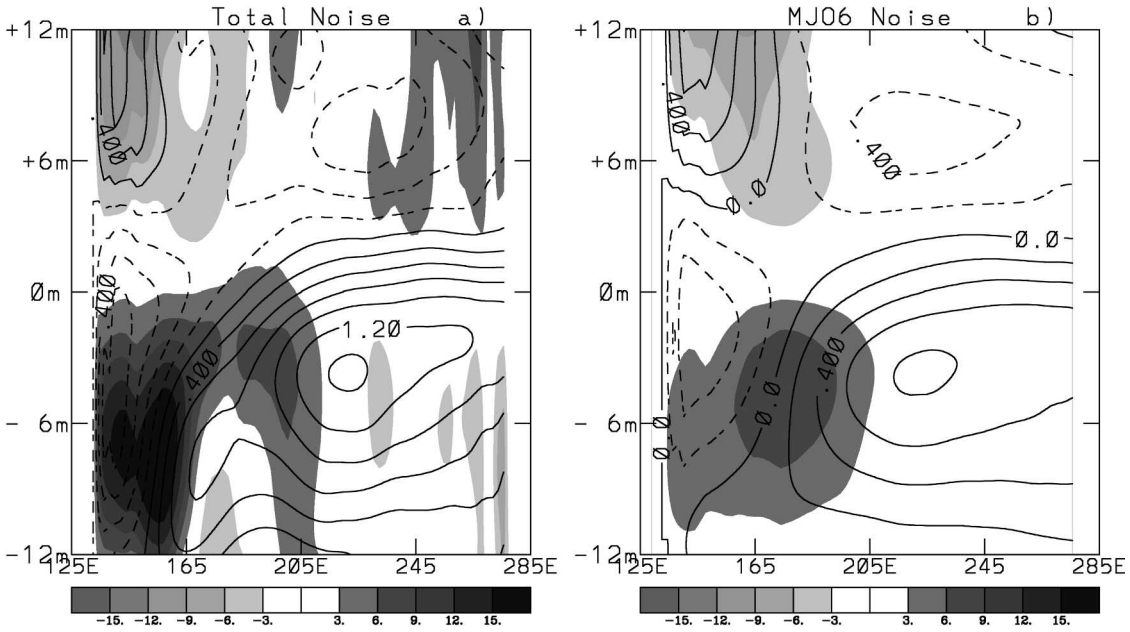

FIG. 12. Regressions of (a) uncoupled zonal stress anomaly (shading) and simulated thermocline anomaly (contours) and (b) MJO6 zonal stress anomaly (shading) and simulated thermocline anomaly (contours) onto the Niño-3 SST index. Fields are averaged in latitude between 5°N and 5°S, and a 90-day running mean was applied prior to the regressions. The shading level is 3×10^{-4} N m^{-2} for stress. The contour interval is 0.1 m for thermocline depth.

duced by the MJO that matter for the evolution of ENSO. Rather, the episodic nature of the MJO results in surface flux variations with a long low-frequency tail. Thus, single or multiple intraseasonal MJO events yield a low-frequency variation of zonal stress or heat flux that can directly drive the coupled system toward either El Niño or La Niño. For instance, Zavala-Garay et al. (2003) reproduced some of the observed ENSO behavior by driving a coupled model (whose ENSO mode was slightly damped) with observed estimates of stochastic zonal stress and heat flux. The implication was that the observed stochastic forcing exhibited a systematic low-frequency variation in association with the observed ENSO cycle.

This result is confirmed by regression of the low-frequency tail (90-day running mean) of our estimate of stochastic zonal stress onto Niño-3 (shading in Fig. 12a). By definition of the stochastic stress, there is near-zero correlation between uncoupled zonal stress and Niño-3 at zero lag. However, 6–8 months prior to the peak of Niño-3, uncoupled westerly stress anomalies are evident in the far western Pacific. These uncoupled stress anomalies are small (~1/10) compared to the coupled stress anomaly associated with ENSO (Fig. 11). However, they drive a response in the thermocline (elevated to the west and suppressed to the east) that peaks 3–4 months before Niño-3. The MJO6 component of this uncoupled stress accounts for less than half of this low-frequency behavior of the uncoupled stress, but it accounts for nearly two-thirds of the resultant thermocline perturbation (Fig. 12b). Again, this emphasizes that the large spatial scale of the MJO makes it an especially efficient driver of equatorial thermocline variability.

This low-frequency thermocline variation driven by the noise (Fig. 12) is conducive to the subsequent development of El Niño. Though these thermocline perturbations are small (~1 m), they may be amplified by coupling and may be sufficient to constrain ENSO variability in some weakly damped models (e.g., Zavala-Garay et al. 2003). The issue is raised again as to whether this low-frequency zonal stress variability is truly noise or whether it is an artifact of trying to develop the noise from a limited observational record. Nonetheless, the result of Zavala-Garay et al. (2003), whereby the observed Niño-3 behavior was recovered from a coupled model driven by an observed estimate of the noise, appears to be explained. Weak, uncoupled westerly stress anomalies in the western Pacific, predominately resulting from the low-frequency behavior of the MJO, systematically occur some 6–8 months prior to El Niño.

5. Conclusions

This study has explored the temporal and spatial characteristics of the uncoupled (or noise) component

of atmospheric variability and has examined how they relate to ENSO. This stochastic component is defined as that part of atmospheric variability that is linearly unrelated to weekly mean Indo–Pacific SSTs at zero lag. Our justification for using this definition is based on the slow evolution of SST and the fast adjustment time (order of a few days) of the atmosphere responding to SST. Hence, stochastic noise is given as the statistically uncoupled atmospheric variability.

To extract this noise component from the total atmosphere fields (e.g., OLR, surface winds), the part of the atmospheric circulation that is potentially predictable (e.g., using a coupled dynamical forecast model) as a result of slowly varying SSTs is removed. This atmosphere–ocean coupled component is defined as the atmosphere anomaly (annual cycle removed) that is linearly related to the first nine EOFs of SST anomaly. A majority of low-frequency atmospheric variability is accounted for by this coupled component. However, some low-frequency power, which is especially relevant to driving a response in the equatorial thermocline, is captured in the noise components of both OLR and surface wind. It is also clear that the MJO is retained entirely within the noise component. EOF analysis of the noise components reveals the MJO to be the dominant mode of variability. This result is significant because previous modeling studies involving stochastic atmospheric forcing do not discern a dominant time scale to the forcing (Blanke et al. 1997; Neelin et al. 2000; Zavala-Garay et al. 2003). This discrepancy is not important in model studies where the ENSO dynamics are quasi linear because it is only the low-frequency tail of the noise that can project onto the ENSO mode (e.g., Roulston and Neelin 2000; Zavala-Garay et al. 2003). However, dominance of MJO variability in the noise may be important when more realistic models of the coupled climate, which explicitly simulates coupled intraseasonal variability, are used to investigate ENSO variability.

Forcing a linear ocean model provides further evidence of the importance of the correct representation of the MJO within this atmospheric noise component. Intraseasonal Kelvin waves are efficiently excited by the presence of the MJO over the western Pacific Ocean. In fact, up to 70% of the simulated equatorial model thermocline variance is accounted for by the MJO forcing. The equatorial ocean acts as a selective low-pass filter, responding most efficiently to the forcing that projects onto the gravest Kelvin waves. Hence, the largest response occurs for the lower-frequency component of the MJO. The observed seasonal variability of the MJO, with peak activity in austral summer, is transmitted to the variance of the eastern Pacific thermocline through the forcing of Kelvin waves. The phase locking of ENSO to the annual cycle, combined with the importance of the timing of western Pacific surface wind forcing in determining the amplitude of ENSO (Bergman et al. 2001; Fedorov 2002; Zhang and Gottschalck 2002; Fedorov et al. 2003), suggests that this is an important point to be considered when more realistic models are used to study atmospheric noise forcing.

The noise was also found to be a strong function of the state of ENSO. For the observed record considered here (1982–99), westerly surface anomalies and warm SSTs first appear in the western Pacific some 8 months before El Niño peaks. As El Niño develops, these westerly anomalies and warm SST slowly shift eastward toward the central Pacific, and the far western Pacific cools. Concurrently, the uncoupled zonal wind variance exhibits a similar evolution, migrating from the west to the central Pacific Ocean, following the warmest SSTs. This may be a sign that separating weather noise from coupled processes in a complex coupled environment is not a simple task. The evolution of the uncoupled component exhibits coupled characteristics in that it is impossible to tell whether the state of the ocean is due to the noise forcing or if the ocean is in fact determining the character of the noise. On the other hand, it does suggest that the noise could be simply parameterized to be a function of the state of ENSO. The tight coupling of the noise to the state of ENSO also explains why incorporation of the observed estimate of noise into a simple ENSO model results in interannual variability that bears some semblance to that observed (Zavala-Garay et al. 2003). Nevertheless, noise-forced variability of the thermocline in the central Pacific Ocean does increase in the months leading up to an El Niño. Examination of the MJO component of the noise reveals that it accounts for less than half of this low-frequency behavior of the stress but does account for nearly two-thirds of the resultant thermocline perturbation. It is again implied that more complex coupled models should include realistic low-frequency behavior of the MJO, which has clear relevance to the evolution of ENSO.

This notion is further supported by examination of observed SST variations in the eastern Pacific in relation to the thermocline variability driven by the observed noise. Eastern Pacific SSTs are observed to warm some 40–60 days after eastward-propagating westerly stress anomalies in the western Pacific excite downwelling Kelvin waves. The warming commences upon arrival of the Kelvin wave in the east Pacific. The relation between wind forcing in the west and SST warming in the east depends on the ocean selectively

responding to the low-frequency tail of the MJO: little relationship between eastern Pacific SST and western Pacific stress is found if all intraseasonal variability is considered. The warming that commences with arrival of the downwelling Kelvin wave also exhibits a longer time scale than that of the Kelvin wave itself. This is suggestive of a coupled feedback, but further diagnosis is beyond the scope of this simple study. Nonetheless, the MJO appears to be the critical component in the link between stochastic weather noise and ENSO.

Acknowledgments. This work commenced while the lead author was a summer intern at CDC, Boulder, Colorado, in 2000. Their hospitality is gratefully acknowledged. We thank K. Weickmann for his interest in this work and for many enlightening discussions. S. Power, C. Zhang, O. Alves, and two anonymous reviewers provided valuable comments on earlier versions of the manuscript. Support was provided by the Centre for Global Atmospheric Modelling, Reading, United Kingdom.

REFERENCES

Bergman, J. W., H. H. Hendon, and K. M. Weickmann, 2001: Intraseasonal air–sea interactions at the onset of El Niño. *J. Climate,* **14,** 1702–1719.

Blanke, B., J. D. Neelin, and D. Gutzler, 1997: Estimating the effect of stochastic wind stress forcing on ENSO irregularity. *J. Climate,* **10,** 1473–1487.

Burgers, G., M. A. Balmaseda, F. C. Vossepoel, G. J. van Oldenborgh, and P. J. van Leeuwen, 2002: Balanced ocean-data assimilation near the equator. *J. Phys. Oceanogr.,* **32,** 2509–2519.

Eckert, C., and M. Latif, 1997: Predictability of a stochastically forced hybrid coupled model of El Niño. *J. Climate,* **10,** 1488–1504.

Fedorov, A. V., 2002: The response of the coupled tropical ocean–atmosphere to westerly wind bursts. *Quart. J. Roy. Meteor. Soc.,* **128,** 1–23.

——, S. L. Harper, S. G. Philander, B. Winter, and A. Wittenberg, 2003: How predictable is El Niño? *Bull. Amer. Meteor. Soc.,* **84,** 911–919.

Gill, A. E., 1980: *Atmosphere–Ocean Dynamics.* Academic Press, 662 pp.

Harrison, D. E., and B. S. Giese, 1988: Remote westerly wind forcing of the eastern equatorial Pacific: Some model results. *Geophys. Res. Lett.,* **15,** 804–807.

Hendon, H. H., B. Liebmann, and J. Glick, 1998: Oceanic Kelvin waves and the Madden–Julian oscillation. *J. Atmos. Sci.,* **55,** 88–101.

——, C. Zhang, and J. Glick, 1999: Interannual variation of the Madden–Julian oscillation during austral summer. *J. Climate,* **12,** 2538–2550.

Jin, F.-F., 2001: Low-frequency modes of tropical ocean dynamics. *J. Climate,* **14,** 3874–3881.

Kalnay, E., and Coauthors, 1996: The NCEP/NCAR 40-Year Reanalysis Project. *Bull. Amer. Meteor. Soc.,* **77,** 437–471.

Kessler, W. S., 2001: EOF representations of the Madden–Julian oscillation and its connection with ENSO. *J. Climate,* **14,** 3055–3061.

——, 2002: Is ENSO a cycle or a series of events? *Geophys. Res. Lett.,* **29,** 2125, doi:10.1029/2002GL015924.

——, and R. Kleeman, 2000: Rectification of the Madden–Julian oscillation into the ENSO cycle. *J. Climate,* **13,** 3560–3575.

——, M. J. McPhaden, and K. M. Weickmann, 1995: Forcing of intraseasonal Kelvin waves in the equatorial Pacific. *J. Geophys. Res.,* **100,** 10 613–10 631.

Lengaigne, M., J. P. Boulanger, C. Menkes, G. Madec, P. Delecluse, E. Guilyardi, and J. Slingo, 2003: The March 1997 westerly wind event and the onset of the 1997/98 El Niño: Understanding the role of the atmospheric response. *J. Climate,* **16,** 3330–3343.

Liebmann, B., and C. A. Smith, 1996: Description of a complete (interpolated) outgoing longwave radiation dataset. *Bull. Amer. Meteor. Soc.,* **77,** 1275–1277.

McPhaden, M. J., 2002: Mixed layer temperature balance on intraseasonal timescales in the equatorial Pacific Ocean. *J. Climate,* **15,** 2632–2647.

Meinen, C., and M. J. McPhaden, 2000: Observations of warm water volume changes in the equatorial Pacific and their relationship to El Niño and La Nina. *J. Climate,* **13,** 3551–3559.

Moore, A. M., and R. Kleeman, 1999: Stochastic forcing of ENSO by the intraseasonal oscillation. *J. Climate,* **12,** 1199–1220.

Neelin, J. D., F.-F. Jin, and H.-H. Syu, 2000: Variations in ENSO phase locking. *J. Climate,* **13,** 2570–2590.

North, G. R., T. L. Bell, R. F. Cahalan, and F. J. Moeng, 1982: Sampling errors in the estimation of empirical orthogonal functions. *Mon. Wea. Rev.,* **110,** 699–706.

Penland, C., and P. D. Sardeshmukh, 1995: The optimal growth of tropical sea surface temperature anomalies. *J. Climate,* **8,** 1999–2024.

Philander, S. G., 1990: *El Niño, La Nina, and the Southern Oscillation.* Academic Press, 293 pp.

Prabhakara, C., D. A. Short, and B. E. Vollmer, 1985: El Niño and atmospheric water vapor: Observations from Nimbus 7 SMMR. *J. Climate Appl. Meteor.,* **24,** 1311–1324.

Reynolds, R. W., and T. M. Smith, 1994: Improved global sea surface temperature analyses using optimum interpolation. *J. Climate,* **7,** 929–948.

Roulston, M. S., and J. D. Neelin, 2000: The response of an ENSO model to climate noise, weather noise, and intraseasonal forcing. *Geophys. Res. Lett.,* **27,** 3723–3726.

Salby, M. L., and H. H. Hendon, 1994: Intraseasonal behavior of clouds, temperature, and motion in the Tropics. *J. Atmos. Sci.,* **51,** 2207–2224.

Shinoda, T., and H. H. Hendon, 2002: Rectified wind forcing and latent heat flux produced by the Madden–Julian oscillation. *J. Climate,* **15,** 3500–3508.

——, H. H. Hendon, and J. Glick, 1998: Intraseasonal variability of surface fluxes and sea surface temperature in the tropical western Pacific and Indian Oceans. *J. Climate,* **11,** 1685–1702.

Takayabu, Y. N., T. Iguchi, M. Kachi, A. Shibata, and H. Kanzawa, 1999: Abrupt termination of the 1997–98 El Niño in response to a Madden–Julian oscillation. *Nature,* **402,** 279–282.

Thompson, C. J., and D. S. Battisti, 2000: A linear stochastic dynamical model of ENSO. Part I: Model development. *J. Climate,* **13,** 2818–2832.

Vecchi, G. A., and D. E. Harrison, 2000: Tropical Pacific sea surface temperature anomalies, El Niño, and equatorial westerly wind events. *J. Climate,* **13,** 1814–1830.

Wang, B., and X. Xie, 1998: Coupled modes of the warm pool climate system. Part I: The role of air–sea interaction in maintaining Madden–Julian Oscillation. *J. Climate,* **11,** 2116–2135.

Wheeler, M. C., and H. H. Hendon, 2004: An all season real-time multivariate MJO index: Development of an index for monitoring and prediction. *Mon. Wea. Rev.,* **132,** 1917–1932.

Zavala-Garay, J., A. M. Moore, C. Perez, and R. Kleeman, 2003: The response of a coupled model of ENSO to observed estimates of stochastic forcing. *J. Climate,* **16,** 2827–2842.

Zhang, C., 1997: Intraseasonal variability of the upper-ocean thermal structure observed at 0° and 165°E. *J. Climate,* **10,** 3077–3092.

——, and J. Gottschalck, 2002: SST anomalies of ENSO and the Madden–Julian oscillation in the equatorial Pacific. *J. Climate,* **15,** 2429–2445.